

Chiral dynamics of nuclear matter at finite temperature¹

S. Fritsch ^a, N. Kaiser ^a and W. Weise ^{a,b}

^a Physik Department, Technische Universität München, D-85747 Garching, Germany

^b ECT*, I-38050 Villazzano (Trento), Italy

email: nkaiser@physik.tu-muenchen.de

Abstract

We extend a recent calculation of nuclear matter in the systematic framework of chiral perturbation theory to finite temperatures T . The contributions from one- and two-pion exchange diagrams which cause nuclear binding and saturation at $T = 0$ are included for $T > 0$ in the density and temperature dependent free energy per particle, $\bar{F}(\rho, T)$. The calculated pressure isotherms display the familiar first-order liquid-gas phase transition of isospin symmetric nuclear matter with a critical point at $T_c \simeq 24$ MeV and $\rho_c \simeq 0.08$ fm⁻³. While T_c is somewhat higher than the typical values given in the literature, the emerging overall picture is remarkably close to more elaborate multi-parameter calculations. We also consider pure neutron matter at $T > 0$ in the same framework and find fair agreement with sophisticated many-body calculations for neutron densities $\rho_n < 0.2$ fm⁻³.

PACS: 12.38.Bx, 21.65.+f

Keywords: Effective field theory at finite density and temperature; Liquid-gas phase transition of nuclear matter; Neutron matter at finite temperature.

The analysis of data from low-energy heavy-ion collisions in the regime of nuclear fragmentation has lead to the picture that heated nuclear matter undergoes a first-order phase transition from a liquid-like state to a vaporized gas state [1, 2]. This liquid-gas phase transition of isospin symmetric nuclear matter is in fact very similar to that of the familiar van-der-Waals gas, with a corresponding critical temperature of $T_c \simeq (16 - 18)$ MeV [2] and a critical density of $\rho_c = (0.06 - 0.07)$ fm⁻³ [2]. Clearly, the dynamical description of this phase transition is an important topic in any microscopic calculation of nuclear matter. In the $\sigma\omega$ -mean field model of Serot and Walecka [3] nucleons are described as Dirac-quasiparticles moving in self-consistently generated scalar and vector mean fields and a critical temperature of $T_c \simeq 19$ MeV is typically found [4]. As an other example, the sophisticated many-body calculations of the Urbana group [5] using the V14 effective NN-interaction (plus an adjustable 3N-interaction) predict a critical temperature of $T_c \simeq 18$ MeV [5].

In a recent work [6], we have used chiral perturbation theory for a systematic treatment of the nuclear matter many-body problem. In this calculation the contributions to the energy per particle, $\bar{E}(k_f)$, originate exclusively from one- and two-pion exchange between nucleons and they are ordered in powers of the Fermi momentum k_f (modulo functions of k_f/m_π). It has been demonstrated in ref.[6] that the empirical saturation point and the nuclear matter compressibility $K \simeq 255$ MeV can be well reproduced at order $\mathcal{O}(k_f^5)$ in the chiral expansion

¹ Work supported in part by BMBF, GSI and DFG.

with just one single momentum cut-off scale of $\Lambda \simeq 0.65$ GeV which parametrizes the necessary short range dynamics. Most surprisingly, the prediction for the asymmetry energy, $A(k_{f0}) = 33.8$ MeV, is in very good agreement with its empirical value. Furthermore, as a nontrivial fact pure neutron matter is predicted to be unbound and the corresponding equation of state agrees roughly with that of sophisticated many-body calculations for low neutron densities $\rho_n \leq 0.25$ fm $^{-3}$. In a subsequent work [7], the momentum and density dependent single-particle potential $U(p, k_f)$ (i.e. the average nuclear mean field) has been calculated in the same framework. It was found that chiral 1π - and 2π -exchange give rise to a potential depth for a nucleon at the bottom of the Fermi sea of $U(0, k_{f0}) = -53.2$ MeV. This value is in very good agreement with the depth of the empirical optical model potential and the nuclear shell model potential.

Given the fact that many properties of nuclear matter can be well described by chiral πN -dynamics treated (perturbatively) up to three loop order it is natural to consider in a further step finite temperatures T in order to check whether the first-order liquid-gas phase transition of nuclear matter is reproduced by this particular dynamics. Such an investigation is the subject of the present paper.

For the relatively low temperatures $T \leq 30$ MeV which are of interest in this context one can safely neglect effects from thermal pions or thermally excited nucleon-antinucleon pairs. As a consequence, nucleons can be treated non-relativistically and the new parameter, the temperature T , enters only through the nucleons' thermal occupation probabilities given by a Fermi-Dirac distribution.

In ref.[6] the diagrammatic calculation of the energy density at $T = 0$ (as a function of the particle density) has been organized in the number of so-called medium insertions. The latter is a technical notation for the difference between the vacuum and in-medium nucleon propagator (see eq.(3) in ref.[6]). The thermodynamically consistent extension of such an ordering scheme to finite temperatures is to relate it directly to the free energy density $\rho \bar{F}(\rho, T)$, since its natural thermodynamical variables are the particle density ρ and the temperature T . In that case the free energy density of isospin symmetric nuclear matter consists of a sum of convolution integrals of the form,

$$\begin{aligned} \rho \bar{F}(\rho, T) = & 4 \int_0^\infty dp_1 p_1 \mathcal{K}_1 d(p_1) + \int_0^\infty dp_1 \int_0^\infty dp_2 \mathcal{K}_2 d(p_1) d(p_2) \\ & + \int_0^\infty dp_1 \int_0^\infty dp_2 \int_0^\infty dp_3 \mathcal{K}_3 d(p_1) d(p_2) d(p_3), \end{aligned} \quad (1)$$

with the corresponding kernels \mathcal{K}_j to be specified. The quantity

$$d(p_j) = \frac{p_j}{2\pi^2} \left[1 + \exp \frac{p_j^2 - 2M\tilde{\mu}}{2MT} \right]^{-1}. \quad (2)$$

denotes the density of nucleon-states in momentum space. It is the product of the temperature dependent Fermi-Dirac distribution and a kinematical prefactor $p_j/2\pi^2$ which has been included in $d(p_j)$ for convenience. $M = 939$ MeV stands for the (free) nucleon mass. The particle density ρ is calculated from the density of states in momentum space as

$$\rho = 4 \int_0^\infty dp_1 p_1 d(p_1) = -\sqrt{2} \left(\frac{MT}{\pi} \right)^{3/2} \text{Li}_{3/2}(-e^{\tilde{\mu}/T}), \quad (3)$$

and this relationship determines the dependence of the effective one-body "chemical potential" $\tilde{\mu}(\rho, T)$ on the thermodynamical variables ρ and T . The "true" chemical potential is different

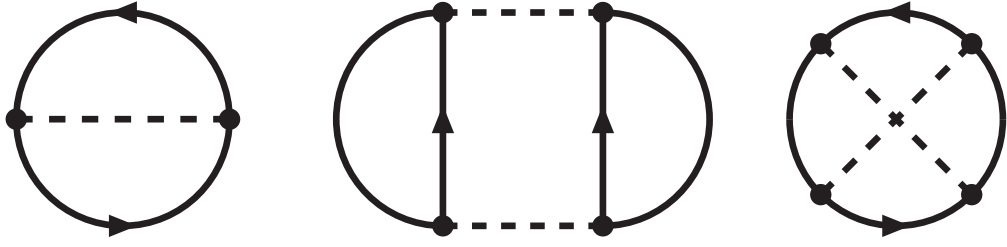


Figure 1: One-pion exchange Fock-diagram and iterated one-pion exchange Hartree- and Fock-diagrams. The combinatoric factor of these diagrams are $1/2$, $1/4$ and $1/4$, in the order shown.

and given by the formula: $\mu = \bar{F} + \rho \partial \bar{F} / \partial \rho$. Note that we are following here closely the approximation scheme introduced in ref.[8]. The infinite series $\text{Li}_\nu(x) = \sum_{k=1}^{\infty} k^{-\nu} x^k$ defines the polylogarithmic function of index ν for $|x| < 1$.

The one-body kernel \mathcal{K}_1 in eq.(1) represents the contribution of the non-interacting nucleon gas to the free energy density and it reads [8],

$$\mathcal{K}_1 = \tilde{\mu} - \frac{p_1}{3} \frac{\partial T_k(p_1)}{\partial p_1} = \tilde{\mu} - \frac{p_1^2}{3M} + \frac{p_1^4}{6M^3}, \quad (4)$$

with $T_k(p_1) = p_1^2/2M - p_1^4/8M^3$ the relativistically improved kinetic energy. The factor 4 in eqs.(1,3) counts the spin-isospin multiplicity of a nucleon.

The contributions to the free energy density $\rho \bar{F}(\rho, T)$ arising from pion-exchange interactions are encoded in the kernels $\mathcal{K}_{2,3}$ in eq.(1). The closed vacuum diagrams related to one-pion exchange (Fock-diagram) and iterated one-pion exchange (Hartree- and Fock-diagrams) are shown in Fig. 1. The 1π -exchange Fock-diagram including the relativistic $1/M^2$ -correction leads to the following contribution to the two-body kernel \mathcal{K}_2 :

$$\begin{aligned} \mathcal{K}_2^{(1\pi)} = & \frac{3g_A^2}{16f_\pi^2} \left\{ 8p_1p_2 - 2m_\pi^2 \ln \frac{m_\pi^2 + (p_1 + p_2)^2}{m_\pi^2 + (p_1 - p_2)^2} + \frac{1}{M^2} \left[-4p_1p_2(p_1^2 + p_2^2) \right. \right. \\ & \left. \left. + m_\pi^2(p_1^2 + p_2^2) \ln \frac{m_\pi^2 + (p_1 + p_2)^2}{m_\pi^2 + (p_1 - p_2)^2} - \frac{2m_\pi^2 p_1 p_2 (p_1^2 - p_2^2)^2}{[m_\pi^2 + (p_1 + p_2)^2][m_\pi^2 + (p_1 - p_2)^2]} \right] \right\}. \end{aligned} \quad (5)$$

As in ref.[6], we choose the value $g_A = 1.3$ for the nucleon axial vector coupling constant, $f_\pi = 92.4$ MeV denotes the weak pion decay constant and $m_\pi = 135$ MeV stands for the (neutral) pion mass. The iterated 1π -exchange Hartree-graph (second diagram in Fig. 1) contributes to the two-body kernel \mathcal{K}_2 with the term:

$$\begin{aligned} \mathcal{K}_2^{(H)} = & \frac{3g_A^4 M m_\pi^2}{8\pi f_\pi^4} \left\{ (p_1 + p_2) \arctan \frac{p_1 + p_2}{m_\pi} \right. \\ & \left. + (p_2 - p_1) \arctan \frac{p_1 - p_2}{m_\pi} - \frac{5}{8} m_\pi \ln \frac{m_\pi^2 + (p_1 + p_2)^2}{m_\pi^2 + (p_1 - p_2)^2} \right\}. \end{aligned} \quad (6)$$

In this expression we have omitted the contribution of a linear divergence proportional to the momentum cut-off Λ (see ref. [6]). All such powerlike terms in Λ are collected in eq.(10). Similarly, the iterated 1π -exchange Fock-graph (last diagram in Fig. 1) gives rise to a two-body

kernel \mathcal{K}_2 of the form:

$$\begin{aligned} \mathcal{K}_2^{(F)} = & \frac{3g_A^4 M m_\pi}{32\pi f_\pi^4} \left\{ 2p_1 p_2 + m_\pi^2 \int_{|p_1-p_2|/2m_\pi}^{(p_1+p_2)/2m_\pi} \frac{dx}{1+2x^2} \right. \\ & \left. \times \left[(1+8x^2+8x^4) \arctan x - (1+4x^2) \arctan 2x \right] \right\}. \end{aligned} \quad (7)$$

The additional diagrams of irreducible 2π -exchange (not shown here, but see Fig. 4 in ref.[6]) generate a contribution to the two-body kernel \mathcal{K}_2 via the expression

$$\mathcal{K}_2^{(2\pi)} = \frac{m_\pi^4}{128\pi^2 f_\pi^4} \left\{ I\left(\frac{p_1+p_2}{2m_\pi}\right) - I\left(\frac{|p_1-p_2|}{2m_\pi}\right) \right\}, \quad (8)$$

with the function

$$\begin{aligned} I(x) = & 3(11g_A^4 - 2g_A^2 - 1) \ln^2(x + \sqrt{1+x^2}) \\ & + 2(g_A^2 - 1) \left[g_A^2(31 + 22x^2) + 5 + 2x^2 \right] x \sqrt{1+x^2} \ln(x + \sqrt{1+x^2}) \\ & + (7 - 2g_A^2 + 91g_A^4)x^2 + (3 + 14g_A^2 - g_A^4)x^4 \\ & + \left[12(15g_A^4 - 6g_A^2 - 1)x^2 + 4(11g_A^4 - 10g_A^2 - 1)x^4 \right] \ln \frac{m_\pi}{2\Lambda}, \end{aligned} \quad (9)$$

obtained from solving the pion-loop integrals. The complete expression for the power divergences specific to cut-off regularization reads:

$$\mathcal{K}_2^{(\Lambda)} = \frac{3\Lambda p_1 p_2}{32\pi^2 f_\pi^4} \left[-10g_A^4 M + (3g_A^2 + 1)(g_A^2 - 1)\Lambda \right]. \quad (10)$$

The term linear in the cut-off Λ stems from iterated 1π -exchange with a contribution of the Hartree- and Fock diagram in the ratio 4 : 1. The term quadratic in the cut-off, on the other hand, originates from irreducible 2π -exchange. Note that this contribution, eq.(10), is fully equivalent to that of a momentum independent NN-contact interaction.

Next, we come to the three-body kernel \mathcal{K}_3 which incorporates the temperature and density dependent Pauli-blocking effects in intermediate NN-states. The iterated 1π -exchange Hartree-graph contributes to the three-body kernel \mathcal{K}_3 in the form:

$$\mathcal{K}_3^{(H)} = \frac{3g_A^4 M}{4f_\pi^4} \int_{|p_1-p_2|}^{p_1+p_2} dq \frac{q^4}{(m_\pi^2 + q^2)^2} \ln \frac{|p_1^2 - p_2^2 + q^2 + 2p_3 q|}{|p_1^2 - p_2^2 + q^2 - 2p_3 q|}, \quad (11)$$

and from the iterated 1π -exchange Fock-graph one finds,

$$\begin{aligned} \mathcal{K}_3^{(F)} = & \frac{3g_A^4 M}{16f_\pi^4} \left\{ \frac{1}{8p_3^3} \left[4p_1 p_3 + (p_3^2 - p_1^2 - m_\pi^2) \ln \frac{m_\pi^2 + (p_1 + p_3)^2}{m_\pi^2 + (p_1 - p_3)^2} \right] \right. \\ & \times \left[4p_2 p_3 + (p_3^2 - p_2^2 - m_\pi^2) \ln \frac{m_\pi^2 + (p_2 + p_3)^2}{m_\pi^2 + (p_2 - p_3)^2} \right] \\ & \left. + \int_{|p_2-p_3|}^{p_2+p_3} dq \frac{q^2}{m_\pi^2 + q^2} \left[\ln \frac{|p_1 + h|}{|p_1 - h|} + \frac{m_\pi^2}{R} \ln \frac{|p_1 R + (p_1^2 - p_3^2 - m_\pi^2)h|}{|p_1 R + (p_3^2 + m_\pi^2 - p_1^2)h|} \right] \right\}, \end{aligned} \quad (12)$$

with the abbreviations:

$$R = \sqrt{(m_\pi^2 + p_1^2 - p_3^2)^2 + 4m_\pi^2(p_3^2 - h^2)}, \quad h = \frac{1}{2q}(p_2^2 - p_3^2 - q^2). \quad (13)$$

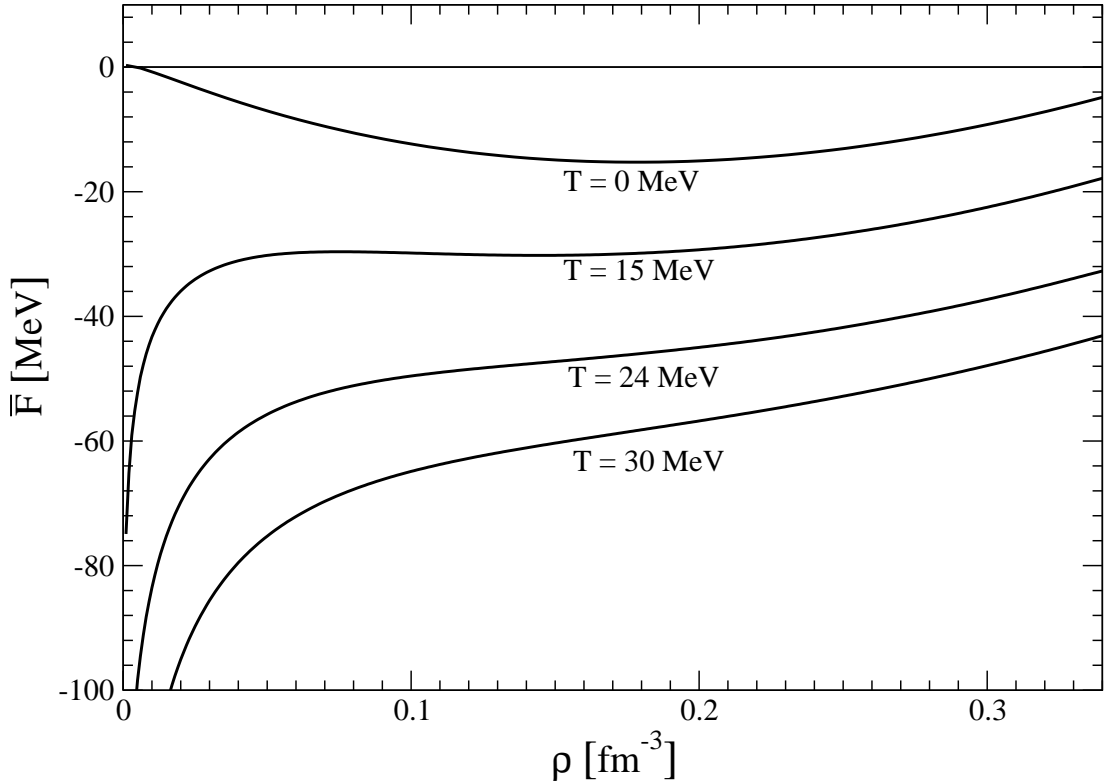


Figure 2: The free energy per particle of isospin symmetric nuclear matter $\bar{F}(\rho, T)$ versus the nucleon density ρ . Each curve is labeled with its corresponding constant temperature T .

Note that all integrands in representations of $\mathcal{K}_{2,3}$ are odd functions of their respective integration variable and therefore one could even drop the absolute magnitude on the lower integration limits.

Via general thermodynamical relations [4] one finally derives from the free energy per particle $\bar{F}(\rho, T)$ the pressure $P(\rho, T)$ and the entropy per particle $\bar{S}(\rho, T)$ as:

$$P(\rho, T) = \rho^2 \frac{\partial \bar{F}(\rho, T)}{\partial \rho}, \quad \bar{S}(\rho, T) = -\frac{\partial \bar{F}(\rho, T)}{\partial T}. \quad (14)$$

We are now in the position to present numerical results for isospin symmetric nuclear matter at finite temperatures. We use consistently the same parameters as in our previous work [6]. There, our only parameter, the cut-off scale $\Lambda = 646.3 \text{ MeV} \simeq 7f_\pi$, has been fine-tuned to the binding energy per particle, $-\bar{E}(k_{f0}) = 15.26 \text{ MeV}$. Fig. 2 shows the free energy per particle $\bar{F}(\rho, T)$ as a function of the nucleon density ρ for various temperatures $T = 0, 15, 24, 30 \text{ MeV}$. The uppermost line is the attractive branch of the nuclear matter saturation curve at $T = 0$. The singular behavior of the free energy per particle $\bar{F}(\rho, T)$ for $\rho \rightarrow 0$ at $T > 0$ is a generic feature (see e.g. the figures and tables corresponding to the results of the Urbana group in ref.[5]). The internal energy per particle $\bar{F}(\rho, T) + T \bar{S}(\rho, T)$, on the other hand, approaches approximately the value $3T/2$ for $\rho \rightarrow 0$.

Fig. 3 shows the calculated pressure isotherms $P(\rho, T)$ of isospin symmetric nuclear matter. As it should be these curves display a first-order liquid-gas phase transition similar to that of the van-der-Waals gas. The coexistence region between the liquid and the gas phase (which has

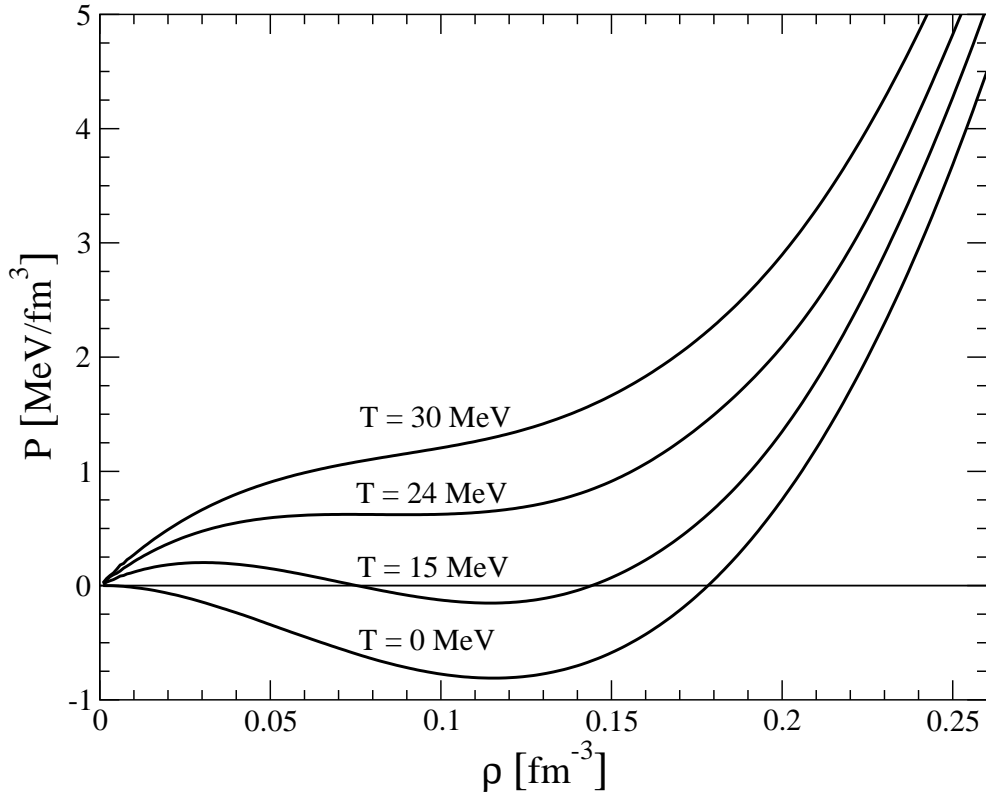


Figure 3: Pressure isotherms in isospin symmetric nuclear matter. The coexistence region of the liquid and gas phase ends at the critical point $\rho_c \simeq 0.08 \text{ fm}^{-3}$ and $T_c \simeq 24 \text{ MeV}$.

to be determined by the Maxwell construction [4]) terminates at the critical temperature T_c . From there on the pressure isotherms $P(\rho, T)$ grow monotonically with the particle density ρ . In the present calculation we find a critical temperature of $T_c \simeq 24 \text{ MeV}$ and a critical density of $\rho_c \simeq 0.08 \text{ fm}^{-3} \simeq 0.45\rho_0$ (with $\rho_0 = 0.178 \text{ fm}^{-3}$, the predicted nuclear matter saturation density). While the critical density ρ_c and the critical pressure $P(\rho_c, T_c) \simeq 0.62 \text{ MeV fm}^{-3}$ are in good agreement with most other calculations, the predicted critical temperature $T_c \simeq 24 \text{ MeV}$ is somewhat too high. Physically interpreted this means that in our calculation heated nuclear matter stays too long in the liquid phase in which the nucleons on the average attract each other more strongly than in the gas phase. Therefore the slightly high value of T_c may point to some missing short range NN-repulsion. Note however that the zero-range approximation of any such short range NN-repulsion is effectively already taken into account in the present calculation via eq.(10), since the cut-off Λ has been adjusted to the empirical binding energy per particle. Interestingly, the nuclear matter saturation curve at $T = 0$ (see Fig. 5 in ref.[6]) agrees very well with the sophisticated many-body calculation of ref.[5] up to quite high densities and therefore does not give any hint on missing short range NN-repulsion. Despite the somewhat too high critical temperature $T_c \simeq 24 \text{ MeV}$, it is certainly gratifying to observe that perturbative chiral pion-nucleon dynamics (treated up to three-loop order) reproduces basic features of the first-order liquid-gas phase transition of isospin symmetric nuclear matter.

The present calculation is readily adapted to the case of pure neutron matter at finite temperatures T . Only the isospin factors of the pion-exchange diagrams (see Fig. 1) change when switching from isospin symmetric nuclear matter to pure neutron matter. The free energy

per neutron $\bar{F}_n(\rho_n, T)$ takes a form analogous to eq.(1), namely:

$$\begin{aligned} \rho_n \bar{F}_n(\rho_n, T) = & 2 \int_0^\infty dp_1 p_1 \mathcal{K}_1 d(p_1) + \int_0^\infty dp_1 \int_0^\infty dp_2 \mathcal{K}_{n,2} d(p_1) d(p_2) \\ & + \int_0^\infty dp_1 \int_0^\infty dp_2 \int_0^\infty dp_3 \mathcal{K}_{n,3} d(p_1) d(p_2) d(p_3). \end{aligned} \quad (15)$$

The neutron density $\rho_n = \rho/2$ gets reduced by a factor 2 in comparison to ρ calculated via eq.(3) and the same applies to the one-body term proportional to \mathcal{K}_1 in eq.(15). The contributions from 1π -exchange and iterated 1π -exchange to the neutron kernels $\mathcal{K}_{n,j}$ are determined by certain relative isospin factors as,

$$\mathcal{K}_{n,2}^{(1\pi)} = \frac{1}{6} \mathcal{K}_2^{(1\pi)}, \quad \mathcal{K}_{n,j}^{(H)} = \frac{1}{12} \mathcal{K}_j^{(H)}, \quad \mathcal{K}_{n,j}^{(F)} = -\frac{1}{6} \mathcal{K}_j^{(F)}, \quad (j = 2, 3), \quad (16)$$

while irreducible 2π -exchange leads to the expression

$$\mathcal{K}_{n,2}^{(2\pi)} = \frac{m_\pi^4}{768\pi^2 f_\pi^4} \left\{ I_n\left(\frac{p_1 + p_2}{2m_\pi}\right) - I_n\left(\frac{|p_1 - p_2|}{2m_\pi}\right) \right\}, \quad (17)$$

with the modified function

$$\begin{aligned} I_n(x) = & 3(19g_A^4 - 2g_A^2 - 1) \ln^2(x + \sqrt{1 + x^2}) \\ & - 2 \left[g_A^4(26x^2 - 7) + 2g_A^2(13 + 10x^2) + 5 + 2x^2 \right] x \sqrt{1 + x^2} \ln(x + \sqrt{1 + x^2}) \\ & + (19 + 118g_A^2 - 257g_A^4)x^2 + (3 + 14g_A^2 - 9g_A^4)x^4 \\ & + \left[12(1 + 6g_A^2 - 15g_A^4)x^2 - 4(13g_A^4 + 10g_A^2 + 1)x^4 \right] \ln \frac{m_\pi}{2\Lambda}. \end{aligned} \quad (18)$$

The expression for the power divergences specific to cut-off regularization changes accordingly in the case of pure neutron matter,

$$\mathcal{K}_{n,2}^{(\Lambda)} = -\frac{\Lambda p_1 p_2}{64\pi^2 f_\pi^4} \left[2g_A^4 M + (3g_A^2 + 1)(g_A^2 - 1)\Lambda \right]. \quad (19)$$

In Fig. 4, we show by the full lines the calculated free energy per neutron $\bar{F}_n(\rho_n, T)$ for temperatures $T = 10, 20$ MeV. The dashed lines in Fig. 4 correspond to the many-body calculation of the Urbana group [5]. These curves should be considered as a representative of the host of existing neutron matter calculations which scatter around them. In order to demonstrate the effects of the nn -interaction, we show by the dotted lines in Fig. 4 the result of a free neutron gas. One observes a fair agreement of our calculation with the results of ref.[5] for low neutron densities, $\rho_n \leq 0.2 \text{ fm}^{-3}$. One may also conclude from Fig. 4 that the parameterfree interaction effects generated by chiral 1π - and 2π -exchange are fairly realistic in this low density region.

In summary, we have extended our recent three-loop calculation of nuclear matter in chiral perturbation theory to finite temperatures T . The contributions from one- and two-pion exchange diagrams are included in the density and temperature dependent free energy per particle $\bar{F}(\rho, T)$. This guarantees thermodynamical consistency and the correct $T = 0$ limit to the energy per particle $\bar{E}(k_f)$. We reproduce the familiar liquid-gas phase transition of isospin symmetric nuclear matter. The predicted critical point, $T_c \simeq 24$ MeV and $\rho_c \simeq 0.08 \text{ fm}^{-3}$, lies however somewhat too high in temperature. This may point to some missing short distance (but finite range) NN-repulsion for which the nuclear matter saturation curve at $T = 0$ gave no hint. Furthermore, we have considered pure neutron matter at finite temperatures T in the same framework. We have found fair agreement with sophisticated many-body calculations for the low neutron densities, $\rho_n \leq 0.2 \text{ fm}^{-3}$, relevant for conventional nuclear physics.

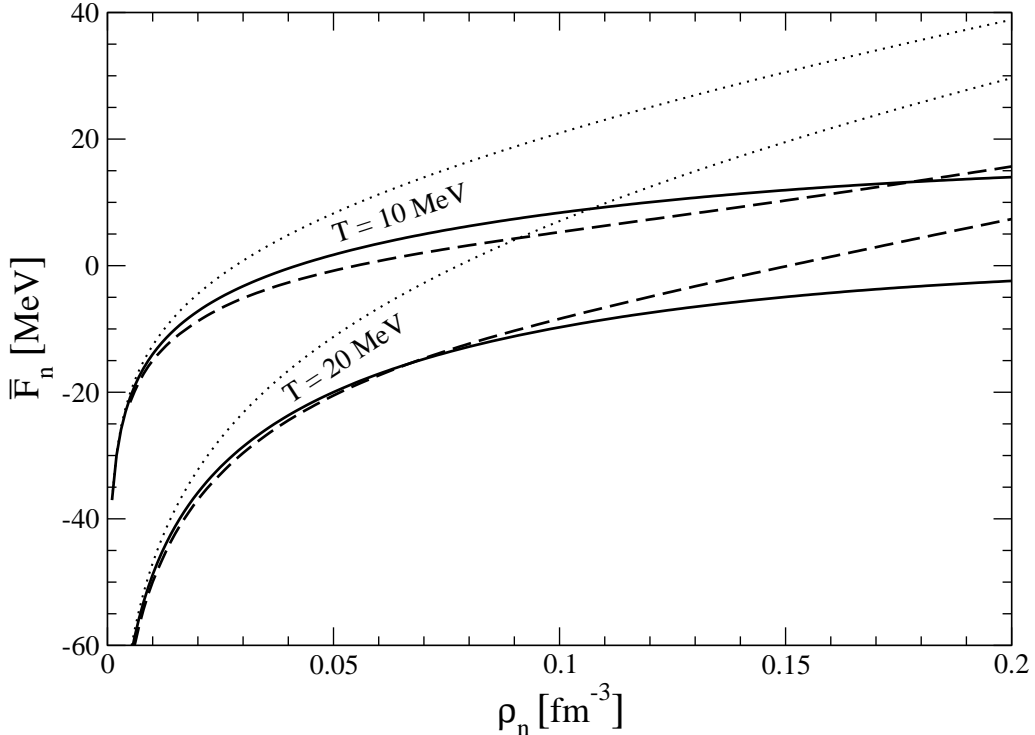


Figure 4: Free energy of pure neutron matter. The full lines give the result of chiral one- and two-pion exchange. The dashed lines correspond to the many-body calculation of ref.[5] and the dotted lines show the result for a non-interacting neutron gas.

References

- [1] L.B. Csernai and J.I. Kapusta, *Phys. Reports* **131** (1986) 223; and refs. therein.
- [2] D. Durand, E. Suraud and B. Tamain, "Nuclear Dynamics in the Nucleonic Regime", Institute of Physics Publishing, Bristol and Philadelphia, 2001; and refs. therein.
- [3] B.D. Serot and J.D. Walecka, *Adv. Nucl. Phys.* **16** (1986) 1; and refs. therein.
- [4] J.I. Kapusta, "Finite-temperature Field Theory", Cambridge University Press, 1989, chapt. 10.
- [5] B. Friedman and V.R. Pandharipande, *Nucl. Phys.* **A361** (1981) 502.
- [6] N. Kaiser, S. Fritsch and W. Weise, *Nucl. Phys.* **A697** (2002) 255.
- [7] N. Kaiser, S. Fritsch and W. Weise, *Nucl. Phys.* **A700** (2002) 343; [nucl-th/0108010](http://arxiv.org/abs/nucl-th/0108010).
- [8] A. Lejeune, P. Grange, M. Martzolff and J. Cugnon, *Nucl. Phys.* **A453** (1986) 189.